

# Search for Low-Dimensional Chaos in Observational Data

J. R. Buchler

Physics Department, University of Florida, Gainesville, Florida, USA

International School of Physics "Enrico Fermi", Course CXXXIII  
"Past and Present Variability of the Solar-Terrestrial System:  
Measurement, Data Analysis and Theoretical Models"  
Eds. G. Cini Castagnoli & A. Provenzale.

## I. INTRODUCTION

Time-dependent signals reveal much more about their sources than do static ones. Thus, the period of a pendulum gives us information about the ratio of the inertia and the restoring force. Frequently, a Fourier spectral analysis of a time-dependent signal displays steady peaks that are indicative of several independent physical frequencies. Such information is of course extremely useful, not only in helping us model the phenomenon, but also in narrowing down the model parameters. The question naturally arises whether we might also be able to extract similar constraints from *unsteady temporal signals*.

All real life systems are very high dimensional (they have a very large number of 'degrees of freedom'), such as well developed turbulence. Often though, the observed behavior is dominated by a few degrees of freedom. In that case we may represent these most important of these with a low dimensional dynamics and hide our ignorance about the other ones by treating them as a stochastic component. In some cases we even get lucky and be able to ignore the stochastic component all together. This lecture concerns itself with this type of situation.

Of course, in real systems one is further plagued by extrinsic physical and observational noise. How large a level of noise is admissible depends on many factors, not the least of which is the nature of the dynamical system itself.

If the dynamics is stationary (autonomous system) and the signal is not multi-periodic, then it must be chaotic. Sometimes the time-dependence is much slower than the variability of the source, and for practical purposes we may consider the system to be stationary. We refer the student to the many excellent introductions to chaos [1], [2], [3] that abound in the literature.

Another difficulty of principle arises. In variable star Astronomy, for example, we generally have access only to the magnitude of the star (The magnitude is defined as the log of the luminosity  $m = -2.5\text{Log}L$ ). Can we ever hope to extract information about the D-dim dynamics from such a *scalar* time-series. The answer is perhaps astonishingly, but fortunately, affirmative.

Although the topic is relatively new there are good introductory books and articles available on the problem of extracting a dynamics from a time-series, for example [4] [5] [6].

## II. THE UNDERLYING DYNAMICS

Suppose a physical system can be described by an autonomous system of ordinary differential equations (ODEs) with  $d$  physical variables that make up the vector  $\mathbf{Y}$ .

$$d\mathbf{Y}/dt = \mathbf{G}(\mathbf{Y}), \quad (2.1)$$

(A more complicated higher order system of ODEs can always be cast into this canonical form). We call this system a  $d$ -dimensional dynamics. With given initial conditions, the solution  $\mathbf{Y}$  of these ODEs, i.e. the  $d$ -dimensional vector of the *physical phase space* that is referred to as the trajectory in physical phase-space.

In most real situations we are unable to measure  $\mathbf{Y}(t)$ . In fact, we usually measure *only one* quantity, say  $m(t)$ . (In the case of variable stars this would naturally be the luminosity or perhaps the radial velocity.) This observable is generally a complicated and unknown function of  $m(\mathbf{Y})$  of the physical state vector.

We assume that the discrete measurement times  $\{t_n\}$  are equally spaced. When this is not the case we have to interpolate which unfortunately introduces additional noise.

The connection between  $\mathbf{Y}(t)$  and  $\{m_n = m(t_n)\}$  will be made through what is termed a *phase-space reconstruction*. From  $\{m_n\}$  we construct the  $d_E$ -uplets of vectors

$$\mathbf{X}(t_n) = \mathbf{X}^n = \{m(t_n), m(t_n - \Delta), m(t_n - 2\Delta), \dots, m(t_n - (d_E - 1)\Delta)\} \quad (2.2)$$

where the delay  $\Delta$  is an integer times the time-interval. Both the physical space and the reconstruction space are Euclidian ( $d$  and  $d_E$  are integer).

We assume now that these vectors themselves are generated by a  $d_E$ -dim dynamics

$$d\mathbf{x}/dt = \mathbf{g}(\mathbf{x}), \quad (2.3)$$

or equivalently by an  $d_E$ -dim map

$$\mathbf{X}^{n+1} = \mathbf{F}[\mathbf{X}^n], \quad (2.4)$$

It does not matter whether we use the description 2.3 or 2.4 – the two are clearly related with  $\{\mathbf{X}^n = \mathbf{x}(t_n)\}$ . It is natural to assume that the observable  $m$  is a smooth function of the physical phase space variable  $\mathbf{Y}$ , *viz*  $\{m(t_n)\} = \{m(\mathbf{Y}(t_n))\}$ . Thus, for example, we assume that the luminosity of a star is a smooth function of the dynamical variables, such as radii, velocities and temperatures, for example.

A theorem now states that there is a one-to-one (differentiable) relation between the vector function  $\mathbf{Y}(t)$  in the  $d$ -dim physical phase-space and the vector function  $\mathbf{x}(t)$  in the  $d_E$ -dim reconstruction space, provided that  $d_E$  is sufficiently large so that the reconstructed trajectory is devoid of intersections and cusps. When the latter condition is satisfied one says that the reconstruction space is an *embedding space*, and no additional benefit can be gained from further increasing the dimension  $d_E$  (A circle can generically be embedded in 3-D; putting it in 4-D or 5-D does not change the circle). The theorem furthermore states that  $d_E$  *need not be larger than 2 times the fractal dimension of the attractor*, rounded off to the next integer value [7]. In practical time-series, that one need not go to this bound and often  $d_E = d$ . In the following we will loosely refer to the dimension of the reconstruction space as  $d_E$ . Another obvious, but important constraint is that the function  $m(\mathbf{Y})$  preserves all the necessary information about all the degrees of freedom of the dynamics.

This theorem is extremely powerful because some properties are preserved in the embedding, such as the Lyapunov exponents and the fractal dimension [7] [5]. Once the map has been obtained we can thus *infer quantifiable properties of an unknown underlying dynamics from the observations of a single variable*. This is important because often an observational data set is too short or too noisy to allow a *direct* estimation of these quantities. Of the fractal dimensions the Lyapunov dimension  $d_L$  is easiest to calculate, and it is defined in terms of the Lyapunov exponents  $\{\lambda_i\}$  as

$$d_L = K + \frac{1}{|\lambda_{K+1}|} \sum_{i=1}^K \lambda_i \quad (2.5)$$

where the  $\{\lambda_i\}$  are in ordered in decreasing size and  $K$  is the largest integer for which the sum is positive.

The *minimum* embedding dimension of course sets an upper bound on the physical dimension  $d$ . A lower limit is obtained from the obvious fact that a fractal attractor has to be embedded in an integer dimensional space. Thus

$$d_L < K + 1 \leq d_L \leq d_E \quad (2.6)$$

When we are lucky the two limits coincide and we can obtain  $d$ .

It is our aim to find a global representation, as opposed to local representations, of the flow, i.e. a single function  $\mathbf{F}$  that evolves the trajectory according to eq. 2.4 in *all* of phase-space.

We have no a priori knowledge about how to choose the global map  $\mathbf{F}$  (or the flow  $\mathbf{g}$ ). It is however natural to try a polynomial expansion. This is particularly appropriate when the dynamics is only weakly nonlinear, as seems to be the case for example for stellar pulsations [8]. Thus we set

$$\mathbf{F}(\mathbf{X}) = \sum_{k=1}^p \mathbf{C}_k P_k(\mathbf{X}), \quad (2.7)$$

where the polynomials  $P_j(\mathbf{X})$  are constructed to be orthogonal on the data set [9], [10], [11] and  $p$  is the expansion order (typically 4 or 5).

An equivalent approach is to treat the polynomial expansion as a least squares problem, *i.e.* one minimizes the sum  $\mathcal{S}$

$$\mathcal{S} = \sum_{\alpha=1}^{d_e} E_{\alpha} \quad (2.8)$$

$$E_{\alpha} = \sum_n (X_{\alpha}^{n+1} - F_{\alpha}(\mathbf{X}^n))^2 \quad (2.9)$$

$$\mathbf{F}(\mathbf{X}) \equiv \sum_k \mathbf{B}^k \mathcal{M}_k(\mathbf{X}) \quad (2.10)$$

with respect to the vector coefficients  $\mathbf{B}^k$ , where  $\mathcal{M}_k(\mathbf{X})$  represents all the monomials up to order  $p$  that can be formed with the  $d_e$  components  $X_{\alpha}$  of the vectors  $\mathbf{X}$ . The sum over  $n$  runs over the whole data set. In the following we will also use one of the components  $E_{\alpha}$  to measure the error.

Instead of a standard QR least squares algorithm it is better to use a singular value decomposition (SVD) approach to effect the minimization and to obtain the coefficients of the polynomial map [12]. The SVD algorithm has several advantages [13]. First, it is a very stable numerical method and it is more than ten times faster than the Gram-Schmidt procedure. Second, it allows one to introduce a large number of unknown parameters in the fit (even more than there are data points). This is important because the number of parameters goes up very fast with polynomial order  $p$ , as  $(C_p^{p+d_e})$  and other methods such as QR become singular. With SVD the redundant combinations give rise to eigenvalues that fall below the machine error or a self-imposed cut-off  $\omega_c$  value and they are *automatically eliminated*.

### III. A TEST CASE: THE RÖSSLER OSCILLATOR

The system of 3 equations known as the Rössler oscillator [3] is given by

$$\frac{dx_1}{dt} = -x_2 - x_3 \quad (3.1)$$

$$\frac{dx_2}{dt} = x_1 + ax_2 \quad (3.2)$$

$$\frac{dx_3}{dt} = b + (x_1 - c)x_3 \quad (3.3)$$

The dimension of the 'physical' phase-space of the Rössler system is thus  $d=3$ . The Rössler oscillator has been widely studied [3] [14]. In some regions of parameter space  $(a, b, c)$  the trajectory fills what is commonly a Rössler band (It is not really a band but is made out of infinitely fine layers, somewhat like 'pâte feuilletée').

The trajectory of this system is chaotic (*i.e.* one of the Lyapunov exponents is positive and nearby trajectories are divergent) and the attractor is strange (it has a fractal dimension) [2]. Since strange and chaotic behavior seem to occur simultaneously for the systems of interest to us we shall simply refer to the attractor as chaotic.

#### A. The test-data sets

For our tests we have chosen the values  $a=0.2$ ,  $b=0.2$  and  $c=4.8$  in eq. 3.3 for which the solution is chaotic and the attractor is in the shape of a band, the so called 'Rössler band' [14] [3]. In the following, when we talk about the Rössler band or attractor, we refer to the Rössler system with these specific parameter values. Other parameter values give attractors with different properties. For further details of all these tests we refer to Serre et al. [12].

On top in Fig. 1 we show the temporal segment of  $x_1(t)$  that we use as test input data in the nonlinear analysis. (The data sequence has been obtained by integrating the Rössler system with a fourth order Runge-Kutta algorithm with a fine time-step of 0.001.) Since we want to test our method we have specifically chosen a relatively short test-data set of 4000 points with  $\delta t$  chosen so as to give of the order of 60 equally spaced points per 'cycle'.

We stress that this segment of  $x_1$  data which is sampled at regular time-intervals, is all the information that we allow ourselves in the global flow reconstruction, *i.e. we do not use any information about the other two variables,  $x_2(t)$  and  $x_3(t)$ .*

It has been shown that some nonlinear methods can erroneously indicate low dimensional behavior for stochastic data ([15] [16] also cf. the lectures by Provenzale and by Smith in this Volume). It is therefore important that our analysis be able to clearly distinguish between the first, deterministic, and the second, stochastic data sets.

We have thus also created a second, stochastic test-data set as follows [12]. We first 'pre-whiten' the Rössler data set by subtracting the dominant frequency and its 8 harmonics, all with their respective Fourier amplitudes and phases

– we thus split the signal into a periodic and an irregular part. The Fourier spectrum of the irregular component has a broad band structure, and we compute the envelope of its (complex) Fourier spectrum. Then we convolve its inverse Fourier transform with a white noise signal, in other words we create a stochastic signal with the same color as the irregular signal. Finally we mix this colored stochastic signal with the originally subtracted periodic component of the Rössler signal. The resultant stochastic data set is displayed in Fig. 1. Note that, by construction, the envelope of the Fourier spectrum of the stochastic signal is the same as that of the Rössler signal.

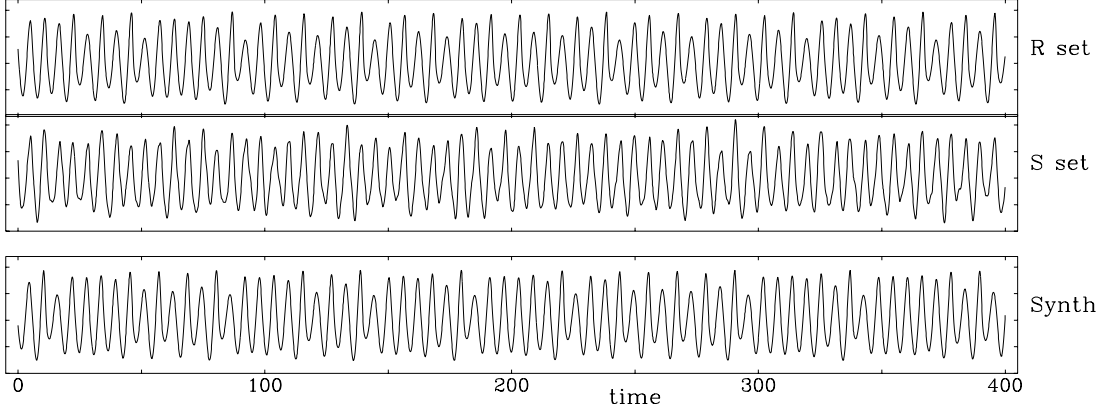


FIG. 1. Input data sets: *top*: Rössler data; *middle*: stochastic data, Reconstructed signal: *bottom*: stochastic data

By eye it is impossible to distinguish between the Rössler and the stochastic data sets. The Fourier spectra do not distinguish either because, by construction, they are very similar. What tools do we have to distinguish between the two signals?

The study of many systems has shown that it is often revealing to make a 'first return map', i.e. to plot one extremum of the signal versus the following one [3] [14]. Fig. 2 compares the first return map for the Rössler (R) and the stochastic (S) signals. Clearly the S signal does not have the coherence of the R signal. The close resemblance of the R map to the logistic map [2] suggests that the Rössler attractor is born out of a cascade of period doublings and that a horseshoe structure underlies its dynamics. We caution though that only very dissipative attractors can give rise to such nice compact first return maps.

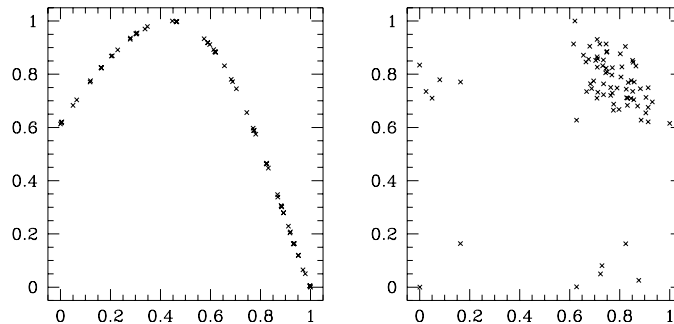


FIG. 2. First return maps: *left*: Rössler data; *right*: stochastic data

While it is of course possible to plot the trajectory in a 3-D picture, this is generally not the optimal type of representation because often the attractor is compressed in some directions. It is preferable to project the trajectory onto Broomhead and King [17] coordinates  $\{\xi_i\}$ . These projections onto the eigenvectors of the correlation matrix have the property of providing an optimal spreading of the attractor in all 'directions'. The first column of Fig. 3 shows the BK projections onto the first three axes for the R signal and the fourth column that of the S signal. Here we see again that the stochastic signal is fuzzier (less coherent).

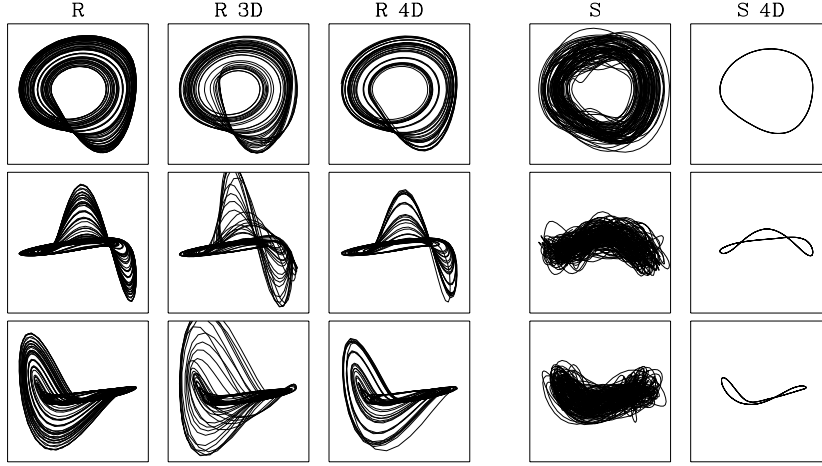


FIG. 3. Broomhead-King projections; *top*:  $\xi_2$  vs  $\xi_2$ , *middle*:  $\xi_1$  vs  $\xi_2$ , *bottom*:  $\xi_2$  vs  $\xi_3$ ; Rössler data, col. 1; Reconstructed signal col. 2 3-D, col. 3 4-D; Stochastic data, col. 4, Reconstructed signal, col. 5

Abarbanel et al. [5] have developed a simple, yet very useful and powerful tool for estimating the embedding dimension, namely the method of 'false nearest neighbors' [18]. The underlying principle is best described by the following analogy: If we defined the distances between stars as being those which we measure on the celestial sphere we would find many nearest neighbors that are 'false' because they merely fall on neighboring lines of sight. We have to go to higher dimension (3 here) to correctly determine the distances. The method of false nearest neighbors generalizes this notion. One computes the distances between points  $\mathbf{X}_n$  in higher and higher embedding dimensions  $d_E$ . When the percentage of nearest neighbors does not change any more with increasing  $d_E$  we have found the minimum embedding dimension.

Fig. 4 displays the percentage of false nearest neighbors as a function of  $d_E$  and the tolerance ([5]), and for two values of the delay parameter  $\Delta$ . The percentages drop off very fast for the R set that is displayed in the two figures on the left, and they indicate that the R data are embeddable in 3-D. The situation is quite different for the S data set shown in cols. 3 and 4, indicating a much larger dimension (as it should because the dimension of a stochastic signal is indeed very large; the percentage still decreases with  $d_E$  because for the small number of data points the density of points decreases so fast with dimension [5]).

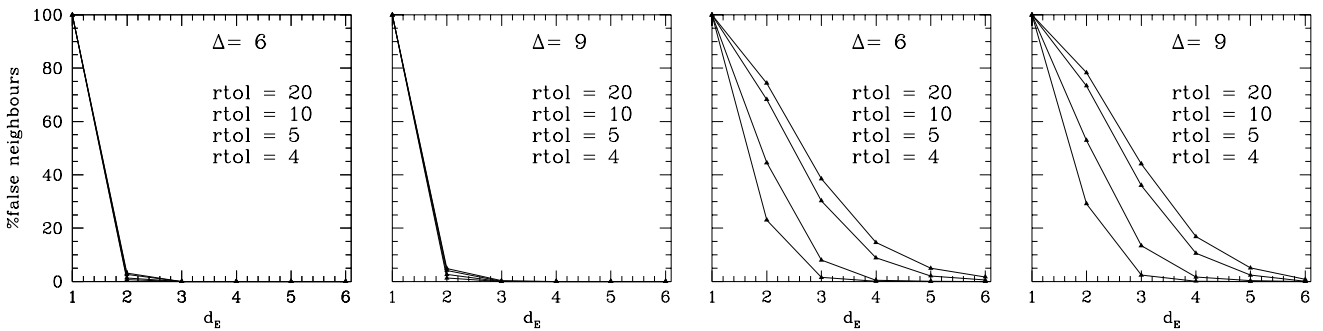


FIG. 4. Percentage of false nearest neighbors: *left*: R signal, *right*: S signal

A totally different characterization of an attractor, of a topological nature, has been discussed in Letellier et al. [19] and, as an example, has been applied to the Rössler band as well. The idea is that a chaotic attractor can be described by the population of unstable periodic orbits, their related symbolic dynamics and their linking numbers. In three dimensional cases, periodic orbits may be viewed as knots and, consequently, they are robust with respect to smooth parameter changes allowing the definition of topological invariants under isotopy (continuous deformation). This topological approach is thus based on the organization of periodic orbits and symbolic dynamics. It is a very

powerful tool, but unfortunately, it only works for attractors for which the first return map consists of relatively well defined branches.

## B. The Flow Reconstruction

We are ready now to discuss the global polynomial flow reconstruction. Our reconstruction contains several unknown parameters: First we have the dimension  $d_E$ . It is of course the minimal value of this parameter that we would like to determine, and we increase  $d_E$  until we obtain an embedding. Next we have the delay  $\Delta$ . Studies of nonlinear time-series have shown that for many purposes there is an optimal time-delay  $\Delta$  that is obtained from mutual information considerations (*e.g.* [4] [5]). However, for our analysis this value is not necessarily the best. For example, too short a delay collapses the attractor onto the diagonal and noise becomes a serious problem, whereas too large a delay causes a very strong nonlinearity in the map, such that a polynomial assumption cannot handle it. We therefore treat  $\Delta$  as a free parameter in our search and anticipate (hope) that there is some range in which a polynomial map works fine. Finally, the parameter  $p$  is the highest order polynomial that we allow in the map. Again since the number of coefficients of the map goes like  $C_{d_e+p}^p$  we would like to keep it to a minimum.

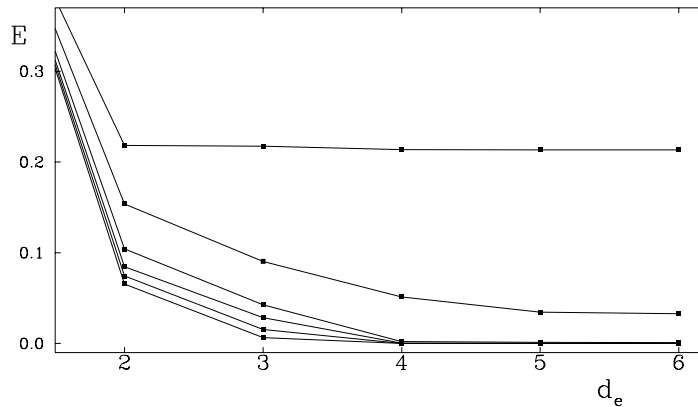


FIG. 5. Error norm as a function of embedding dimension  $d_E$  and polynomial order,  $p=2, \dots, 6$ , increasing from top to bottom

In Fig. 5 we display a typical behavior of the error norm as a function of  $d_E$  and of  $p$  for fixed delay  $\Delta=11$ . We only show the error for the first component  $\alpha=1$  of  $\mathbf{X}$  (*c.f.* eq. 2.10) because the other components behave similarly. As one would expect the error falls off monotonically with polynomial order  $p$ . In 3-D the error norm decreases relatively slowly though. A probable reason is that a low order polynomial approximation to the Rössler map may not be accurate enough (A rational polynomial map might be more appropriate, [9] [20]).

The important result from Fig. 5 is that the norm shows a very clear drop and levelling off at  $d_e$  around 3 and 4. This suggests that we should be able to construct a global map in 4-D, but that it may already be possible to do so in 3-D. This evidence alone is however not sufficient to establish the minimum embedding dimension, and we need to look also at the behavior of the properties of the *synthetic trajectories*. By this we mean trajectories  $\{\mathbf{X}^n\}$  that, once we have constructed the map  $\mathbf{F}$ , we obtain by iteration of eq. 2.4 starting with some seed value  $\mathbf{X}^0$ . We refer to any *component*  $X_\alpha^n$  of these trajectories as a *synthetic signal*. Indeed it might be that the error norm is very small, indicating a good fit, but that the generic trajectories of the map are very different from the test data.

Now a word about Lyapunov exponents (cf. *e.g.* [2]) which give a useful quantitative measure of the map and of its attractor. In the case of the Rössler system where we know the 3 ODEs we can compute the 3 Lyapunov exponents in our chosen  $(a, b, c)$  regime directly – They are found to have the values  $\lambda_1=0.057$ ,  $\lambda_2=0$ ,  $\lambda_3=-4.5$ , and  $d_L = 2.013$ . One notes that one of the Lyapunov exponents of the Rössler system is exactly zero because the system of ODEs is autonomous (a time independent flow) [2]. Next, the presence of a *positive* Lyapunov exponent indicates that the attractor is *chaotic*. Finally, the fractal Lyapunov dimension implies that it is a strange attractor [2].

The question now arises whether it is possible to recover the values of these Lyapunov exponents from the R test data? The answer is two-fold: First, the computation of all of the Lyapunov exponents from a time series necessitates *long* data sets, often at least an order of magnitude longer than is available from observations. Here, for example, the length of our R test-data set (4000) is far too small to yield exponents that come even close to the correct values. In observational data, in addition, noise easily vitiates the reliability of the Lyapunov calculations. Second, however,

we can first construct the map and then generate synthetic trajectories of sufficient length to be able to compute the Lyapunov exponents. The reason why, with this two step procedure, we are not 'getting something for nothing' is discussed in ref. [21].

Table 1 compares these Lyapunov exponents and Lyapunov dimension for synthetic trajectories for various values of embedding dimension and time-delay. In  $d_e \geq 4$  the largest Lyapunov exponents ( $\lambda_1$ ) are seen to be very close to the exact value. An exception occurs for  $d_e=3$  where  $\lambda_1$  and  $\lambda_3$  are too large by a factor of about 2. This fact is probably connected with the relative lack of stability of the map in 3-D. In the next section we shall see that the addition of small amounts of noise stabilizes the map and produces correct Lyapunov exponents. The scatter of the negative exponents is higher than for the positive ones, but this is to be expected [7]. Table 1 shows that, except for  $d_E=3$ , the Lyapunov dimensions are close to their known exact values. For the sampling rate that we use here the exponents are essentially the same whether we compute them for the flow or for the map.

We draw attention to the fact that  $d_L$  is independent of the embedding-dimension  $d_e$ . If our attractor reconstruction is to make sense this is of course a necessary condition, and conversely it is a check on our calculation.

The second Lyapunov exponent  $\lambda_2$  is always very small ( $\approx 10^{-4}$ ). Although we have constructed a map here, the sampling-time is sufficiently small so that the map closely approximates a flow. The smallness of one Lyapunov exponent constitutes a very powerful check on our *a priori* assumption that a flow (eq. 2.4 indeed underlies the dynamics).

As expected there is a range of delays for which one obtains good maps. In Fig. 1, bottom, we show the best synthetic signal (obtained with  $d_E = 4$ ,  $p = 4$ ). It has very similar properties to the original set. (Because the time-series are chaotic, it is not very meaningful to compare them directly. Since the signals are so short, statistical comparison methods are not very useful here either. We therefore have to rely on a number of comparison tests, neither of which is totally convincing by itself, but when taken together they give a good level of confidence [12] [21]. We note here that the Fourier spectrum of the synthetic signal is very similar to that of the R data set. The Broomhead King projections (Fig. 3) are also very similar.

In contrast, the flow reconstruction of the S test data set yields only limit cycles, for all values of  $\Delta$  and  $p$ . In fact the limit cycles are almost identical to the periodic part of the signal. The global flow reconstruction thus recognizes the stochastic noise for what it is and it does not erroneously indicate low dimensional behavior.

### C. Noise

The reconstruction of a stable map encounters some difficulties for the Rössler data set. The reason behind it is that the neighborhood of the attractor is not well described. One can understand this as follows: Suppose we tried to apply this method to system which had a limit cycle. Unless we had a transient we would have no information whatsoever on the neighborhood of the limit cycle, and the neighborhood could equally well come out repulsive or attractive. Noise broadens the attractor and forces the map to form a stable neighborhood.

TABLE 1. Lyapunov exponents and dimension, *left*: R set, *right*: R set + 0.2% gaussian noise

$d_E$	$\Delta$	$\lambda_1$	$\lambda_2$	$\lambda_3$	$\lambda_4$	$\lambda_5$	$d_L$		$d_E$	$\Delta$	$\lambda_1$	$\lambda_2$	$\lambda_3$	$\lambda_4$	$d_L$
exact values:															
		0.057	0	-4.5			2.013								
computed from synthetic signals:															
3	5	0.128	$<10^{-4}$	-6.4			2.020		3	4	0.046	$<10^{-4}$	-17.8		2.003
4	4	0.057		-3.9	-16.7		2.014		3	5	0.041		-16.9		2.003
4	5	0.058		-3.7	-15.0		2.014		3	6	0.055		-16.2		2.003
4	6	0.051		-3.5	-12.7		2.014		3	7	0.062		-14.3		2.004
4	7	0.068		-3.2	-9.0		2.021		4	4	0.063		-17.3	-30.5	2.004
5	4	0.054		-8.0	-19.0	-28.0	2.007		4	5	0.061		-16.8	-28.4	2.004
5	5	0.054		-6.8	-18.2	-28.0	2.008		4	6	0.066		-16.8	-28.5	2.004
5	6	0.055		-5.3	-16.8	-29.0	2.010		4	7	0.068		-15.4	-26.4	2.005
5	7	0.055		-4.8	-15.8	-29.0	2.011								

We conclude from this study (1) that the minimum embedding dimension is 3 and (2) that  $K = \text{int}(d_L)$ . From the inequality (2.6) it thus follows that  $d = 3$ . In other words the global flow reconstruction method recovers the dimension of the dynamical system (3.3) that has generated it.

#### IV. A REAL SYSTEM: THE LIGHT CURVE OF R SCUTI

In 1986 numerical hydrodynamic simulations of metal poor Cepheid models, called W Virginis stars, showed irregular pulsations [22] [23] [24]. A further investigation revealed period doublings as a stellar parameter was varied and concluded that the irregular behavior of these models were a manifestation of low dimensional chaos. These calculations were based on models that ignored convective energy transport and treated radiation transfer in an equilibrium diffusion approximation. In order to confirm the theoretical prediction as to the chaotic nature of the irregular variability it was obviously necessary to compare to observations.

Observationally, it has been known for a long time that the light-curves of W Vir stars are regular (periodic) for low periods, but then develop irregularities as the period and luminosity increase. This increasingly irregular behavior carries over to their more luminous siblings, the RV Tauri stars. Unfortunately, these irregular variables have not received much attention from professional astronomers - the publication of what *appears* to be a table of random numbers is not compatible with career and funding pressures! Hopefully, the development of nonlinear time-series analyses such as this one will change this perception. However the Association of Variable Star Observers (AAVSO) in Cambridge collects observations and compiles data from amateur astronomers around the globe. Often these data are visual, and of poor quality. Yet, the large number of independent measurements make this a wonderful data base. For the variable star R Scuti a large data set of 15 years of data are available. The data have a normal distribution that is independent of magnitude, and it is therefore possible to extract a good light-curve despite the large individual errors. We show a short section of the observational data of R Sct in Fig. 6 together with a smooth fit. It is this fit with equally spaced data points that we use as the input data for our global flow reconstruction. For more details of the smoothing procedure we refer the reader to the original papers [11] [21]. The whole R Sct light-curve is displayed in Fig. 7 on top.

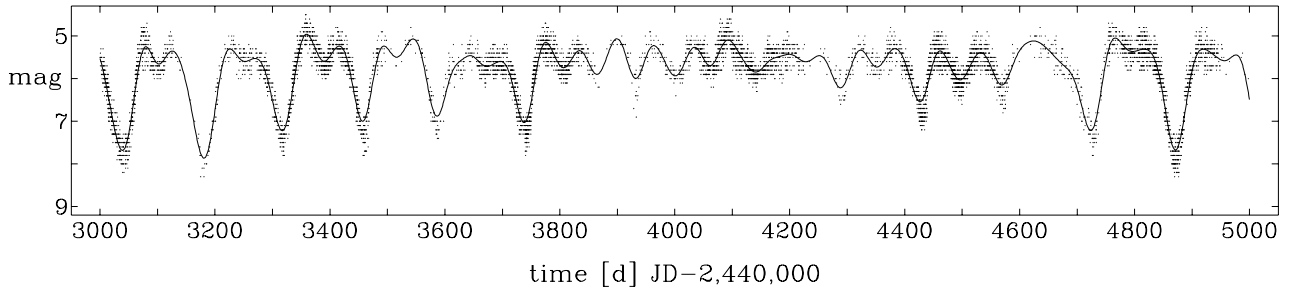


FIG. 6. Typical section of the observational data together with a smooth fit

The Fourier spectral analysis of the light-curve shows a broad dominant peak at  $f \approx 0.007 \text{ d}^{-1}$  and a secondary much broader structure centered on  $f \approx 0.014 \text{ d}^{-1}$ . The analysis of patchy, but very old data going back some 150 years has shown that while the envelope of the Fourier spectrum is more or less steady, the individual peaks are not at all, especially the tertiary ones [25]. There is a further discussion in ref. [21] as to why the light-curve of R Scuti cannot be generated by multiperiodic pulsations, even when evolutionary changes are taken into account.

Space does not permit us to describe the details of the global flow reconstruction and we refer the reader to the original papers [11] [21] (see also [26]).

In Fig. 7, middle and bottom, we exhibit two pieces of synthetic signal (obtained in  $d_E = 4$  with  $p = 4$ ). Visually, the synthetic time-series is very similar to the observational data. The Fourier spectrum similarly has the same envelope.



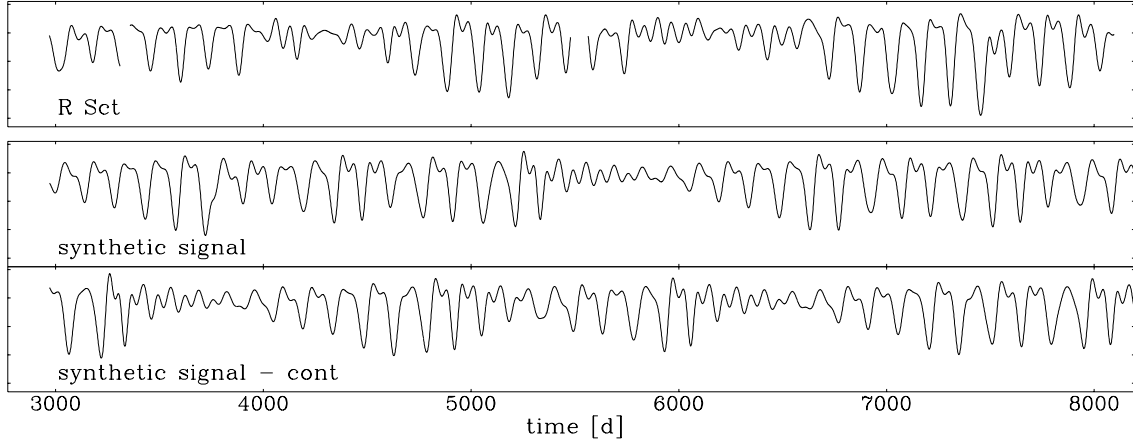


FIG. 7. R Scuti, *top*: Whole light-curve data set used in the analysis, *middle and bottom*: pieces of synthetic light-curves generated with the global map

In Fig. 8 we show the Broomhead-King projections on the lowest three axes. The left-most column represents the observational data. Columns 2 and 3 show our best reconstruction with 4-D and 5-D maps (eq. 2.4). Finally, in col. 4 we show a reconstruction with a flow (eq. 2.3).

In Table 2 we show the Lyapunov exponents and dimension for several values of  $\Delta$  and  $d_E$ . Noteworthy are the following points: (1) the results show a certain robustness with respect to the delay  $\Delta$ , (2)  $d_L \approx 3.1$  is essentially independent of  $d_E$ , (3)  $\lambda_1 > 0$  which establishes the chaotic nature of the attractor, and (4)  $\lambda_2 \approx 0$ , which confirms the presence of a flow. We note that it has been found impossible to construct a map with synthetic signals that bear any resemblance to the data which indicates that the minimum embedding dimension must be greater than 3. However, as Table 2 shows in 4-D we can construct a flow whose properties remain largely invariant as we increase  $d_E$ . We conclude that the minimum  $d_E$  is therefore 4. We add in passing that a false nearest neighbor analysis corroborates 4 as the minimum embedding dimension.

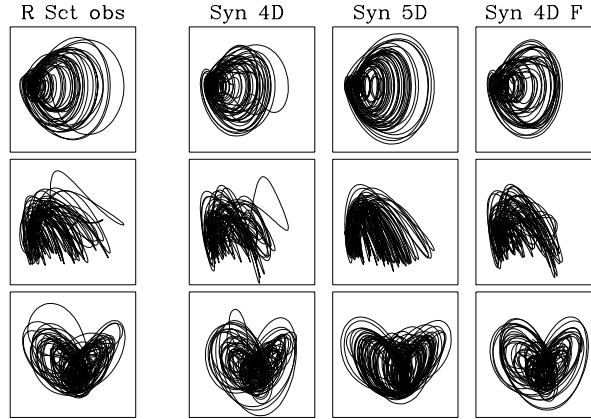


FIG. 8. Broomhead-King projections; *top*:  $\xi_2$  vs  $\xi_2$ , *middle*:  $\xi_1$  vs  $\xi_2$ , *bottom*:  $\xi_2$  vs  $\xi_3$ ; *left*: R Scuti observational data, *cols. 2 and 3*: map reconstructions in 4-D and 5-D, *right*: flow reconstruction in 4-D;

Having now established from the Lyapunov dimension that the lower bound  $K+1$  (rel. 2.6) of the physical phase-space dimension is 4 we thus conclude that  $d = 4$ , i.e. the light-curve of R Scuti is generated by a 4-D dynamics.

---

---

TABLE 2. Lyapunov exponents and dimension, R Scuti

---

---

$d_E$	$\Delta$	p	$\lambda_1$	$\lambda_2$	$\lambda_3$	$\lambda_4$	$d_L$
4	4	4	0.0019	$<10^{-4}$	-0.0016	-0.0061	3.05
4	5	4	0.0017		-0.0014	-0.0054	3.06
4	6	4	0.0019		-0.0009	-0.0051	3.19
4	7	4	0.0020		-0.0011	-0.0052	3.18
4	8	4	0.0014		-0.0010	-0.0049	3.07
5	7	3	0.0016		-0.0005	-0.0041	3.27
6	8	3	0.0022		-0.0003	-0.0018	3.52

---

---

## V. CONCLUSION

The polynomial global reconstruction method has been tested on the Rössler attractor. Using as input a short time-series of only one of the 3 Rössler variables one obtains a very good estimation of the Lyapunov exponents and the fractal dimension of the attractor. Furthermore it is possible to determine that this scalar signal is generated by a 3-D flow (the Rössler equations 3.3), in other words one can find out the dimension of the physical phase-space of the dynamics.

Encouraged by these results the flow reconstruction has been applied to real data, viz the light-curve of the variable star R Scuti. Not only are these data contaminated with a good amount of observational and other extrinsic noise, but we have no a priori information about the dynamics that has generated them.

The analysis has shown that the dynamics which generates the light-curve of R Scuti is of dimension four, i.e. the signal can be generated by a flow in 4-D (eq. 2.1). Furthermore the attractor has a fractal dimension  $\approx 3.1$ . This must be considered remarkable considering that this star undergoes luminosity fluctuations of up to factors of 40 (cf Fig. 1), with shock waves and ionization fronts criss-crossing the stellar envelope. Some of the physical implications have been addressed in references [11] [21].

If nothing else it is interesting that the nature of the irregular variability of these types of stars is no longer a mystery, but that it has such a simple explanation in terms (very) low dimensional chaos.

## ACKNOWLEDGMENTS

It is a pleasure to acknowledge the collaboration of Thierry Serre and of Zoltan Kolláth in the development and application of the global flow reconstruction method. This work has been supported by the National Science Foundation.

- 
- [1] Bergé, P., Pomeau, Y. & Vidal, C. 1984, *Order Within Chaos*, (Wiley: New York).
  - [2] Ott, E. 1993, *Chaos in Dynamical Systems* (Univ. Press: Cambridge).
  - [3] Thompson, J. M. T. & Stewart H. B. 1986, *Nonlinear Dynamics and Chaos* (New York: Wiley).
  - [4] Weigend, A.S & Gershenfeld, N. A. 1994, *Time Series Prediction* (Addison-Wesley: Reading).
  - [5] Abarbanel, H.D.I., Brown, R., Sidorowich, J. J., Tsimring, L. S. 1993, Rev. Mod. Phys. 65, 1331.
  - [6] Letellier, C., Gouesbet, G., LeSceller, L, Brown, R., Buchler, J.R. & Kolláth, Z., 1996, Annals New York Academy of Sciences, in press.
  - [7] Sauer, T., Yorke, J. A. & Casdagli, M. 1991, J. Stat. Phys. 65, 5.
  - [8] Buchler, J. R. 1990b, *NATO ASI Ser. C302*, 1 (Kluwer: Dordrecht).
  - [9] Brown, R. 1992, Orthonormal Polynomials As Prediction Functions In Arbitrary Phase-Space Dimensions, Institute for Nonlinear Science Preprint, UC San Diego.
  - [10] Giona, M., Lentini, F. & Cimagalli, V. 1991, Phys. Rev. A 44, 3496.
  - [11] Buchler, J. R., Serre, T., Kolláth, Z. & Mattei, J. 1995, Phy. Rev. Lett. 74, 842.
  - [12] Serre, T., Kolláth, Z. & Buchler, J. R., 1996, Astronomy & Astrophysics, 311, 833.

- [13] Press, W. H., Teukolski, S. A., Vetterling, W. T. & Flannery, B. P. 1992, *Numerical Recipes* (University Press: Cambridge).
- [14] Packard, N. H., Crutchfield, J. P., Farmer, J. D. & Shaw, R. S. 1980, Phys. Rev. Lett. 45, 712.
- [15] Provenzale, A., Smith, L.A., Vio, R. & Murante, G. 1992, Physica D58, 31.
- [16] Smith, L.A. 1992, Physica D58, 50.
- [17] Broomhead, D. S. & King, G. P. 1987, Physica D 20, 217.
- [18] Kennel, M.B., Brown, R. & Abarbanel, H.D.I. 1992, Phys. Rev. A45, 3403.
- [19] Letellier, C., Gouesbet, G., Soufi, F., Buchler, J.R. & Kolláth, Z., 1996, Chaos, in press.
- [20] Gouesbet, G. 1991a, *Phys Rev.* 43A, 5321.
- [21] Buchler J. R., Kolláth, Z., Serre, T. & Mattei, J. 1996, Ap. J. 462, 489
- [22] Buchler, J.R. & Kovács, G. 1987, Ap. J. Letters, 320, L57
- [23] Kovács G. & Buchler J. R. 1988, *Ap. J.* 334, 971
- [24] Buchler, J. R. 1990a, Annals New York Academy of Sciences, 617, 1.
- [25] Kolláth, Z. 1990, MNRAS 247, 377.
- [26] Buchler, J. R. 1995, Annals New York Academy of Sciences, 773, 1.